Research Article **Open Access**

Marcel Di Vece*, Giorgos Giannakoudakis, Astrid Bjørkøy, and Wingjohn Tang

Luminescent tracks of high-energy photoemitted electrons accelerated by plasmonic fields

DOI 10.1515/nanoph-2015-0029
Received August 5, 2015; accepted November 11, 2015

Abstract: The emission of an electron from a metal nanostructure under illumination and its subsequent acceleration in a plasmonic field forms a platform to extend these phenomena to deposited nanoparticles, which can be studied by state-of-the-art confocal microscopy combined with femtosecond optical excitation. The emitted and accelerated electrons leave defect tracks in the immersion oil, which can be revealed by thermoluminescence. These photographic tracks are read out with the confocal microscope and have a maximum length of about 80 μm, which corresponds to a kinetic energy of about 100 keV. This energy is consistent with the energy provided by the intense laser pulse combined with plasmonic local field enhancement. The results are discussed within the context of the rescattering model by which electrons acquire more energy. The visualization of electron tracks originating from plasmonic field enhancement around a gold nanoparticle opens a new way to study with confocal microscopy both the plasmonic properties of metal nano objects as well as high energy electron interaction with matter.

Keywords: Plasmonics, gold nanoparticle, femtosecond excitation, electron emission, luminescence, confocal microscopy

***Corresponding Author: Marcel Di Vece:** Nanophotonics—Physics of Devices, Debye Institute for Nanomaterials Science, Utrecht University, P.O. Box 80000, 3508 TA Utrecht, The Netherlands, E-mail: m.divece@uu.nl

Giorgos Giannakoudakis, Wingjohn Tang: Nanophotonics—Physics of Devices, Debye Institute for Nanomaterials Science, Utrecht University, P.O. Box 80000, 3508 TA Utrecht, The Netherlands

Astrid Bjørkøy: Department of Physics, Norwegian University of Science and Technology (NTNU), 7491 Trondheim, Norway

1 Introduction

The renewed attention on plasmonics and the current state of characterization technologies such as near field optical microscopy (SNOM) and femtosecond laser spectroscopy are opening up new scientific and technological possibilities in nanophotonics [1, 2]. An important focus in the study of plasmonics is the determination and control of local plasmonic field enhancement by metal nanostructures [3–5]. A remarkable field enhancement of many orders of magnitude has been demonstrated in a Raman spectroscopy study on metal nanostructures [6, 7]. Large optical field enhancement has been observed in narrow gaps between nanoparticles, which is much larger than for a single particle [8–10]. The plasmonic field was imaged by a deflection of the passing electrons in transmission electron microscopy [11], which forms a platform to quantify the local field strength.

The combination of electron photoemission from a metal nanostructure and plasmonic field enhancement revealed photoelectrons with surprisingly high kinetic energies [12–14]. Such high energies are important for various applications such as radiation damage for medical treatment or electron field emission for displays and electron microscopes. The emitted electrons provide important information about the emission process and the plasmonic field. Electron emission can be driven by photoionization (the photoelectric effect [15]), which is a quantum effect, or by the (classical) electric field [16]. The transition between those regimes is characterized by the Keldysh parameter, $\gamma = \omega/\omega_t$, which relates the optical driving frequency ω to a characteristic tunnelling frequency $\omega_t = eF/\sqrt{2m\Phi}$, where F is the electric field, Φ the work function, m the electron mass, and e its charge. When $\gamma \ll 1$, the emission is caused by tunnelling after the electron is accelerated by the optical field. The photoelectrons originating from the metal or dielectric [17, 18] nanostructures follow a quivering motion in the oscillating electromagnetic field and thereby acquire energy. The energy of this electron, also called the ponderomotive potential energy, is determined by the quiver motion in the driving field with a value of $U_p = e^2F^2/4m\omega^2$. Since the ponderomotive potential is

determined by the local field strength, plasmonic field enhancement increases F locally, which can provide an energy of more than a keV (dual pulse) [19].

To date, only photoemitted electrons originating from an individual metal particle or tip have been studied. Extending the study to arrays of small metal particles would enable investigations of the effect of hotspots, often found in the narrow gap between particles or at corners and holes of metal nanostructures: photoemitted electrons may acquire even higher energies.

Confocal laser scanning microscopy (CLSM) allows the optical excitation by femtosecond laser pulses while the luminescence response is recorded simultaneously [20]. The reflection and luminescence from individual nanoparticles can be investigated in a controlled wavelength range. When the photo-emitted electrons interact with their environment, an optical luminescence response could also be measured with this microscope.

In this work, we study the emission of photoelectrons from gold nanoparticles, which were randomly deposited on glass. The randomness ensures that a large range of configurations are created, i.e., providing optimal conditions for hotspots. In a previous work, the electrons were detected by electron spectrometry, which is sensitive to direction and energy. Here we use a CLSM equipped with a femtosecond laser to excite the gold nanoparticles in order for electrons to be released. The interaction of the electrons with the oil matrix creates fluorescent tracks, which can be imaged with the same microscope. Using confocal microscopy to image high-energy particle interaction is unique in its own right. With this approach, the energy and direction of individual emitted electrons and their interaction with matter can be studied. This provides insight in the plasmonic field of the gold nanoparticles under intense and ultrashort illumination.

2 Experimental

The gold nanoparticles were produced by a gas aggregation magnetron sputtering cluster source (NC200U-B, Oxford Applied Research Ltd.) in DC mode with a power of 20 W and Ar flow of 15 sccm [21–23]. The background and operation pressure were 2×10^{-8} and 1.7×10^{-3} mbar, respectively, with a deposition time of 3 min. The gold target had a purity of 99.99%. The particles were deposited on glass substrates, which were cleaned with iso-propanol and sonication.

In this work, we used a state-of-the-art confocal microscope (Leica TCS SP8 MP) equipped with luminescence lifetime system from PicoQuant. The laser used was a high-intensity, linearly polarized Ti:Sapphire fs-laser (Chameleon Vision-S (75 fs) and Vision II (140 fs) from Coherent) and the sample was imaged using an immersion oil objective (60 × NA 1.4, Leica). The immersion oil (Type F, Leica) had a refractive index of 1.5. The confocal microscope only detects light from a thin plane, which is in focus and which has an optical slice thickness of about 500 nm (pinhole was opened to the maximum size). A diffraction limited, monochromatic, polarized beam scans a square area, line by line, pixel by pixel. The Ti:Sapphire laser was operated with an excitation wavelength of 700 nm, a repetition rate of 80 MHz, pulse length of 140 or 75 fs (depending on set up), and a pulse energy of about 30 nJ. The wavelength for luminescence detection using the internal detectors was set from 380 or 410 nm to 650 nm. The photons counted by the single photon avalanche photodiodes (SPAD's) from PicoQuant were passing a band pass filter of 500–550 nm (SPAD 1) and 565–605 nm (SPAD2). A 680 nm short pass filter was used to filter out the excitation laser light. Because of this short pass filter and the chosen detection range only luminescence is detected; reflected light is not measured.

The polarization of the incident laser beam was rotated by use of a half wavelength plate active at 700 nm. A schematic illustration of the gold nanoparticles on the glass sample and the laser beam is shown in Fig 1.

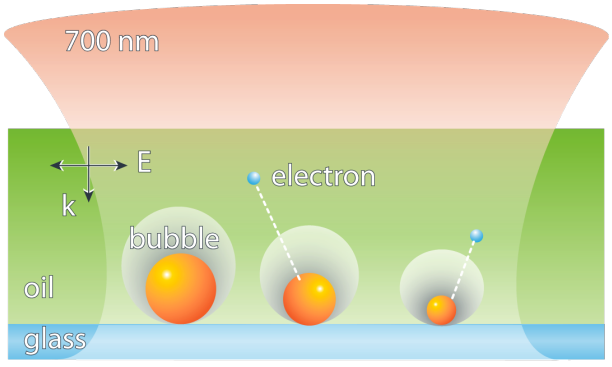

Figure 1: Schematic depiction of gold particles on glass substrate covered with immersion oil. The incident focused fs laser beam creates a nanobubble around the particle and then stimulates the photoemission of an electron, which leaves luminescent defect traces in the oil.

3 Results and Discussion

The particle size ranges from a few nm to about 20 nm with a high fraction at about 15 nm and the areas with gold clusters had a coverage of about 100 to 200 particles/μm^2. From the AFM imaging of the samples, which is shown in the SM, both individual gold nanoparticles and aggregates were observed. Although the gold particle beam from the cluster source is uniform, gold cluster poor areas could be observed, often straight with dimensions of tens of µm. Small patches of the glass surface can become more conductive [24], in this case likely the result from the fabrication method. The conductive glass becomes charged by the sputter gas ions from the cluster source, which exerts a repulsive Coulomb force, which, in turn, diverts the charged gold particles to noncharged parts of the glass.

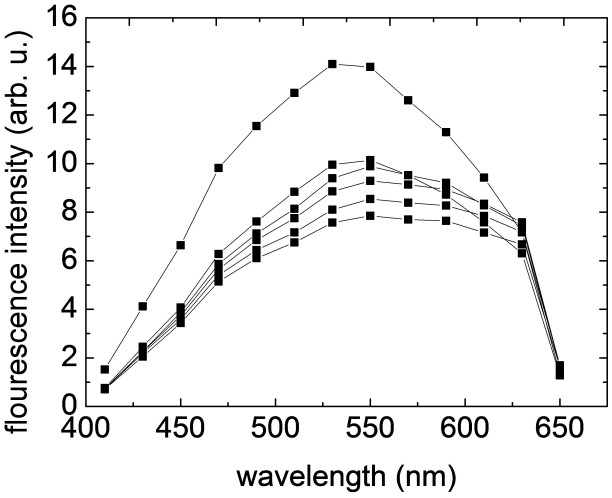

Figure 2: Luminescence spectrum in the range 420 to 650 nm of gold particles on glass as measured by the confocal microscope CLSM with 700 nm pulsed (140 fs) excitation light at times 1, 4, 8, 12, 16 and 20 s. At each consecutive spectrum the intensity decreases and the spectral shape changes. At 650 nm a cut off filter was used.

At first, a spectrum was recorded as a function of time as shown in Figure 2. The spectra have a clear broad peak with an optimum at 530 nm, in agreement with the optical absorption [25] and interband luminescence of gold [26]. Since light of 700 nm was used, the luminescence at lower wavelengths is the result of two-photon excitation. Initially, the luminescence has a high intensity, which drops almost a factor of two after a few seconds of recording (and excitation). The spectral shape changes upon illumination: the contributions in the red become more intense as compared to the peak intensity.

Luminescence recordings in the focal plane as shown in Figure 3 show that immediately from the start of the recording long, thin, straight lines are visible. The fluorescent lines mostly last only one frame, which suggests that the laser beam stimulates the luminescence but also ends it within the time of the frame recording (~1 s). The density of the longer tracks in cluster poor areas is estimated to be 10–30 μm^{-2}, which makes their formation rare events. The fluorescent lines have the same general direction (toward the lower left corner of the image or toward the bottom), depending on the used setup. This indicates that the polarization affects the track direction since this is the only parameter that changes per setup. The length of the fluorescent lines ranges from a few hundred nm to about 80 µm. Although the fluorescent lines often appear straight, slight curvatures and bends within a single fluorescent line can be observed, probably induced by the presence of charge from previous excitation events. In the upper right inset of Figure 3, a zigzag luminescence track is shown, suggesting a more complicated interaction. The luminescent tracks were not observed on glass without gold nanoparticles.

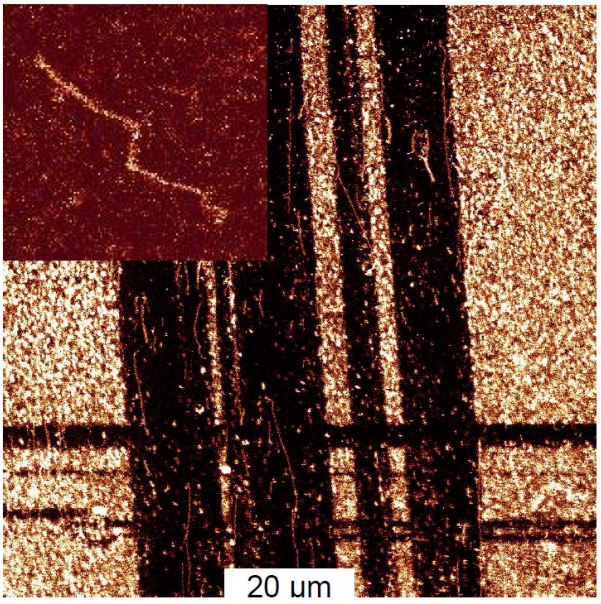

Figure 3: Luminescence scanning image recorded by CLSM of gold particles rich area (bright) gold particle poor area (dark). Pulsed (140 ns) excitation at 700 nm, emission recorded in the range 380–680 nm. Long and shorter luminescence tracks are visible, going toward the lower right. Upper left insert: example of electron track indicating several elastic collisions in the oil medium, which changes its direction considerably.

Sometimes, the end of a fluorescent line is the beginning of following line in the next frame, as shown in Fig-

ure 4. Such fluorescent line sequences were observed to last several frames. Often, fluorescent lines terminate in a small bright spot, which can remain at its position until the end of the experiment. The bright spot is likely the result of the generation of secondary electrons, which produce a considerable amount of defects in the oil. The fluorescent lines have a thickness of one or a few pixels, indicating that the fluorescent source was smaller than the recording pixel size of about 0.15 µm.

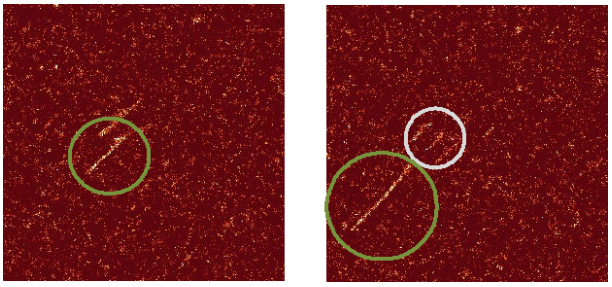

Figure 4: Luminescence in the range of 410–650 nm of gold particles on glass as measured by the confocal microscope CLSM, using pulsed (75 fs) excitation at 700 nm. The images are recorded in sequence (time interval 1.3 s) and the image size is 20 µm. The tracks in the green circles follow each other, while the track in the gray circle is lingering.

The polarization of the incident laser beam was controlled by insertion of a 1/2 wavelength plate, which was rotated 45°. The measurements at three different angles resulted in the three different track directions, which directly follow the polarization of the light as shown in Figure 5A–C. The track angles were measured for the three polarization angles, which show the polarisation dependence of the electron emission process as shown in Figure 5D. In agreement with the field polarization dependence of photo-emitted/accelerated electrons, the direction of the electron tracks is largely directional [27], confirming the light field as the source of the electron emission. This also proves that the tracks are independent of the scanning direction.

In Figure 6, an *XZ* scan, perpendicular to the sample surface, shows luminescence tracks pointing away from the particle decorated surface, into the oil. This demonstrates that the fluorescent tracks are formed in the immersion oil (not in the glass) and that it cannot be a moving particle by lack of a supporting surface.

Based on the arguments of synchronicity and the presence of tracks in the *XZ* scan, the track can only originate from a process prior to the laser hitting a spot on the track. The lines giving rise to luminescence must already be present before the laser reaches the trace. Therefore, the luminescent centers making up the line are created by a process prior to the scan reaching the line and can be formed by local defect generation or ionization in the immersion oil, for which high-energy particles are required. High-energy electrons can be emitted from a plasmonic particle under intense illumination as described in the introduction. However, in previous experiments, the electron acceleration occurred in vacuum in which the electron could move freely. A low atomic density around the gold particle is accomplished by nano-bubble formation during laser incidence [28, 29]. The electron can then accelerate freely inside the nano-bubble before it is emitted as indicated in Figure 1. The nano-bubble forms by a thin vapor layer around the particle, which grows and can become much larger. By increasing the laser power, larger bubbles are formed, which block the experiment. The defects and structural changes that are generated in oil by fast-moving electrons affect the luminescence properties at the positions of their flight path. Subsequently, heat from the incident scanning light beam stimulates luminescence from the defect track, by releasing trapped electrons [30, 31]. A luminescent track along the path of the electron will then become visible. Thermoluminescence occurs in organic substances due to radiative decay of trapped electrons, which are released by thermal stimulation [32, 33]. Quantum mechanical selection rules may only allow thermoluminescence at certain levels of the trapped electron, which may change over time after excitation [34]. In Figure 4A and B, a luminescence track is shown, which is continuing from the end of the previous track, pointing to the time dependence of thermoluminescence. A residual track (gray circle) is also visible, suggesting a lingering effect.

The emitted electron undergoes inelastic scattering, the collision with electrons in the medium, by which energy is lost. This energy loss is typically a few eV up to hundreds of eV and is responsible for the excitation of plasmons and of individual atomic electrons to higher energy levels [35]. Excitation of inner shell electrons requires energies that are generally hundreds or thousands of eV. Such excitations can cause a photoelectron to be emitted after which the ion may relax through Auger decay, in which an electron from a higher level falls down and a further electron is emitted with an energy between 250 eV and 2 keV [36]. Through collisions between the Auger electron and the neighboring atoms, electrons will be liberated, leading to a cascade of ionizations. A study of high-energy electron tracks in photographic emulsions by Herz [37] revealed this phenomenon by the presence of dark spots at the beginning and end of electron tracks. Such spots are

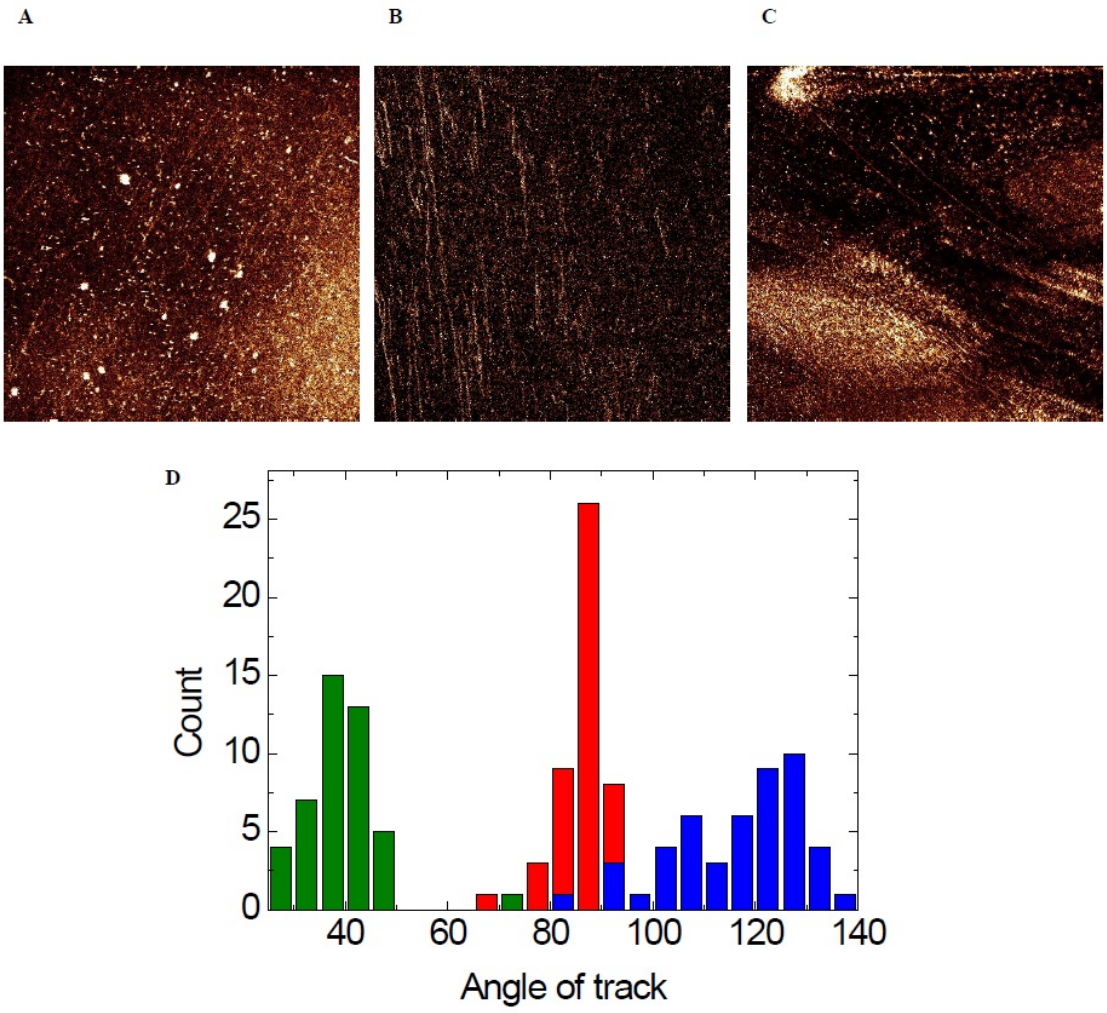

Figure 5: A-C Luminescence image (pulsed (140 fs) excitation at 700 nm. The polarization of the microscope laser beam was changed with a 1/2 wavelength plate. D The angle of the tracks was then measured against the horizontal. The tracks at about 90° (red) are with the system polarization while the tracks under about 40° (green) and 130° (blue) are obtained by rotating the polarization of 45°.

also observed in our experiment and indicate a similar secondary electron emission process.

The electron can also elastically scatter on the core of atoms, which leads to a large scattering angle. The energy transfer is sufficient to displace an atom. This radiation damage, also called *knock-on* or *displacement* damage, is used in medical treatment where controlled damage is desirable [38]. This mechanism is shown in the inset of Figure 3 as an example of an electron scattering under large angles. When the electron has delivered all its kinetic energy it will stop. The termination of a luminescence line could also be caused by an elastic scattering event, after which the electron can move in any direction, making it highly probable that the electron will leave the focal plane and therefore cannot be imaged anymore. Alternatively, electrons moving under an angle with respect to the glass surface will eventually leave the focal plane.

The transfer of energy from a moving electron to the matrix depends on its kinetic energy: at high energies the transfer is low [39] and vice versa. With its initial high energy, the electron therefore first travels in a straight line. When its energy is lowered considerably by inelastic scattering, scattering events become more likely, until it comes to a halt. The scattering of low-energy electrons leads to large angles in the trajectory. A simulation of the scattering process by the Monte Carlo method in the Casino program [40] of energetic electrons in C_2H_6 shows that an energy of about 100 keV is required to obtain straight flight paths of tens of µm. This is in agreement with the NIST database, which lists a stopping range of tens of µm for 100 keV electrons [41]. The electron tracks observed by Herz for ener-

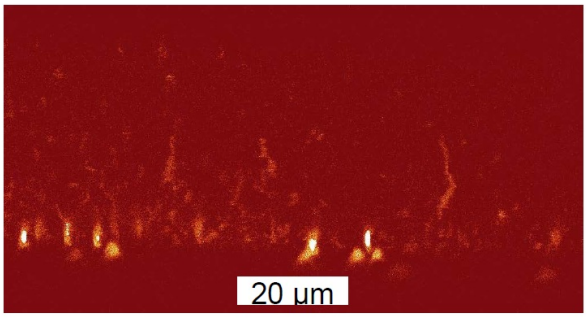

Figure 6: Luminescence image (pulsed (75 fs) excitation at 700 nm, emission recorded in the range 410–650 nm) from a XZ scan, perpendicular to the glass plane. The electron tracks pointing away from the substrate plane are visible inside the immersion oil covering the gold particles. The bright spots along the lower horizon originate from gold particles. The line by line scan starts on the top, confirming that the tracks originate from a prior frame.

gies of about 100 keV have a length of 50 µm. Therefore the luminescence tracks with a length up to 80 µm in this work indicate that the emitted electrons have an initial kinetic energy in the order of 100 keV.

The highest possible energies that electrons can acquire during the emission and acceleration are commonly determined by the cutoff energy, which corresponds to $10 \times U_p$ [42]. For the electron to get a kinetic energy of 100 keV and therefore U_p =10 keV, the electric field around the gold particle or in a gap between gold particles should be about 1.3×10^{10} V/cm. The electric field of the laser light in the focal spot is only about 1.0×10^7 V/cm (30 pJ in an area of about 4×10^4 nm for 140 fs); therefore, in principle, a three-order field enhancement is required to obtain the electric field, which can lead to an electron kinetic energy of 100 keV. The optical absorption cross-section of gold particles with a diameter of 20 nm at resonance is about 300 nm^2[43], which means that most of the light is captured by the particle. Because the laser wavelength (700 nm) is close to the gold nanoparticle plasmon resonance wavelength (> 550 nm), one photon absorption can excite the plasmon. The local field enhancement of a single gold particle depends on its dielectric environment and can be about tens of times for a single particle and much larger for gaps between particles. However, the three-order field enhancement is likely not required as electrons with higher energy than the cutoff energy are also emitted.

The release of high-energy electrons can be produced by a rescattering effect of the electron driven by the electric field on the ionic core, which causes a dephasing by which the electron absorbs energy from the field [44]. This produces electrons with a much larger energy than the ponderomotive energy, with decreasing probability for larger energies. In the rescattering model by Saalman et al. [45] the energy gain of the electron in a potential is caused by laser-field-driven acceleration in a quasistatic cluster potential. The electrons acquire a high transit velocity, which leads to an energy gain that is proportional to the square root of the scattering potential well depth. Since the gold particles in this work are electrically isolated, the repeated scans of the microscope will quickly positively charge the gold nanoparticles by electron emission. The charging of the gold nanoparticles increases the potential well depth and could therefore explain a higher kinetic energy then $10 \times U_p$. Moreover, the acquired kinetic energy increases with increasing particle size.

Fennel et al. [27] showed that the electron can also acquire more energy from the polarization field produced from plasmon oscillations. This process of surface plasmon assisted rescattering in particles produces a preferential ejection of fast electrons along the laser polarization axis, in agreement with the experimental results of this work. Although the larger electron kinetic energies have much lower probability, they can still occur according to these mechanisms. Dual pulse excitation produces higher electron kinetic energies up to $100 \times U_p$ [19, 46], however, the time between pulses in this experiment was too long to benefit from such an effect. It nevertheless demonstrates that with specific conditions, such high energies are, in principle, possible. In good agreement with the experiments of this work, the emission anisotropy increases with energy and is maximum for the most energetic electrons [19].

Despite the lower emission probability of the high-energy electrons, they require less plasmonic field enhancement and make the necessary electron kinetic energy plausible. Therefore the longest electron tracks correspond to the upper limit (and lowest probability) of available plasmonic energy of the gold nanoparticle.

The high laser intensity and absorbed energy in the gold nanoparticle are known to create damage to the particles [14, 47], and by thermal stimulations cause slow movement, which also occurs in this work as observed from the change in the fluorescent pattern. However, the particles will have enough time to emit high-energy electrons before they are too severely damaged or aggregated and the process stops. Because thermoluminescence provides a long life time to the electron track, it is possible to measure them originating from the first instances of the illumination.

Luminescence lifetime imaging microscopy (FLIM) of the particles both the *xy* and *xz* scanning modes (Figure 7) show that fluorescent life times of the order of nanoseconds are present. In the *XZ* scan, a fluorescent halo is visi-

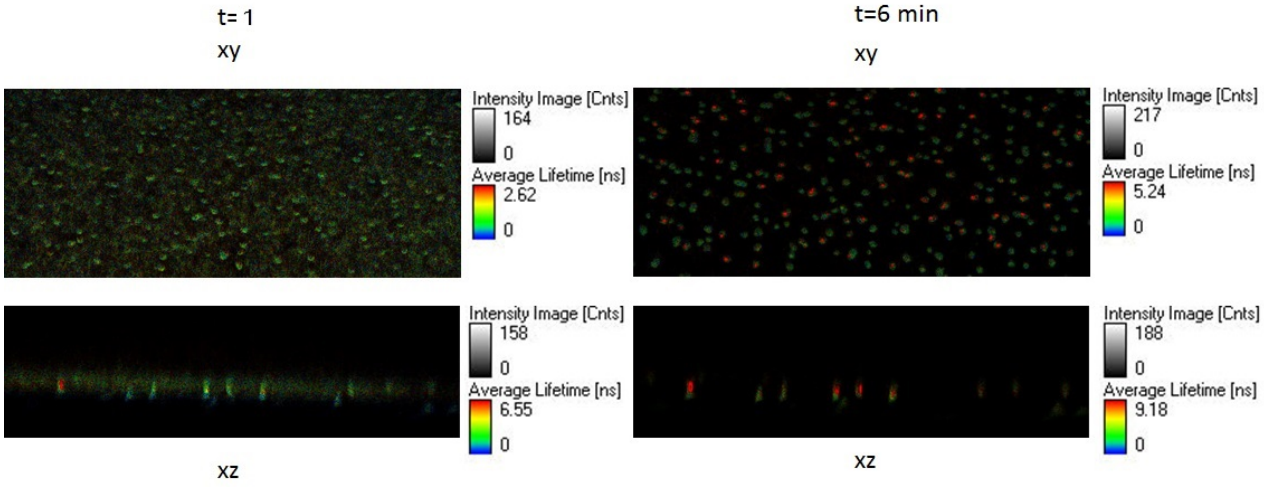

Figure 7: Fluorescent lifetime image microscopy (FLIM) in xy (top) and xz (bottom) scanning mode, accumulating photons for $t = 1$ and $t = 6$ min. The horizontal size is 60 µm. The color scales with the luminescence lifetime while the intensity scales with photon counts. At $t = 1$ the lifetime (a few ns) distribution is spatially more uniform and more intense than at $t = 6$ min.

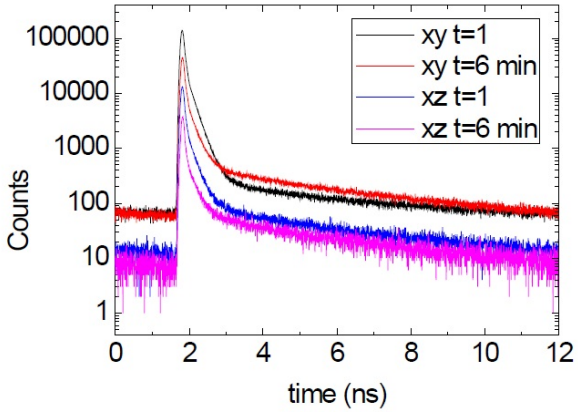

Figure 8: Average lifetime curves of the luminescence in xy and xz scanning mode for t=1 and t=6 min.

ble with lifetimes in the order of a nanosecond. Due to the short life time of the tracks, their collective presence could be measured only by accumulation, giving rise to the haze. The luminescence lifetime of gold particles is in the order of picoseconds to femtoseconds [26]. Therefore, the luminescence in the oil with much longer lifetimes has to originate from the electron-induced defects.

The average lifetime curves corresponding to the images of Figure 7, shown in Figure 8, could be fitted with a third order exponential with the lifetimes of about 40 ps, 0.2 ns and 3.2 ns. The contribution of the 40 ps component reduces about a factor 3 after fs illumination, likely because the gold becomes inactivated by charging, removal, or aggregation. In contrast to the *xy* scan, in the *xz* scan, the contribution of the 3.2 ns component, due to the oil defects, increases by a factor 2 after 6 min. This is a sign that the defect luminescence becomes more important in this scanning mode. In both experiments, the 0.2 ns component reduces by a factor 3 after 6 min, confirming the overall decreasing luminescence. The nanosecond lifetime luminescence confirms that the strong luminescence originates from the oil, likely induced by defects and measured by thermoluminescence. The thermoluminescene of defects also has a low signal with long lifetime (> tens of ns), which correspond to transitions with low probability. Such transitions become more important at the later stages of the process as can be seen from the higher intensity of the decay in Figure 8 for the *XY* scan after 6 min of excitation.

4 Conclusions

In conclusion, fluorescent tracks originating from gold particles on glass are the result of electron emission and plasmonic acceleration. High energies can be provided to the electron by the intense plasmonic field and the rescattering process by which the driven electron is directed around the positively charged core. By (in-)elastic scattering, the moving electron transfers its energy to the oil matrix, leading to the creation of defects, ionization, and trapped electrons. The track becomes visible during the subsequent scan by thermoluminescence, which radiatively releases trapped electrons. The track direction could be controlled by changing the polarization of the exciting light beam. The imaging of such electron tracks opens the way to investigations of plasmonic field enhancement

with optical (confocal) microscopy. By optimizing the local field enhancement, electron kinetic energies of MeV may be achievable. This study demonstrates a new way to create such high-energy electrons, which could be used to produce controlled damage for lithography and medical purposes.

Acknowledgement: Stimulating discussions with Bernd von Issendorff, Dries van Oosten, and Marijn van Huis are appreciated. The Imaging Centre Essen (IMCES) is thanked for making their Leica TCS SP8 Multi-Photon Microscope available. The microscopy assistance by Anthony Squire is very much appreciated. Akshatha Mohan is thanked for TEM assistance. This work has been supported by a Marie Curie Career Integration Grant, Project No: 293687.

Supplementary Material: Detailed information about the samples and Casino simulation of electron trajectories are described.

References

[1] Ozbay, E. Merging Photonics and Electronics at Nanoscale Dimensions. Science 2006;311:189-193.
[2] Novotny L. Hecht, B.; Principles of Nano-Optics, Cambridge University Press, 2008.
[3] Kauranen, M. Zayats, A.V. Nonlinear plasmonics. Nat. Photon. 2012;6:737.
[4] Deeb, C. Zhou, X. Miller, R. Gray, S.K. Marguet, S. Plain, J. Wiederrecht, G.P. Bachelor, R. Size Dependence of the Plasmonic Near-Field Measured via Single-Nanoparticle Photoimaging. J. Phys. Chem. C 2012;116:24734-24740.
[5] Ciracě, C. Hill, R.T. Mock, J.J. Urzhumov, Y. Fernández-Domínguez, A.I. Maier, S.A. Pendry, J.B. Chilkoti, A. Smith, D.R. Probing the Ultimate Limits of Plasmonic Enhancement. Science 2012;337:1072-1074.
[6] Nie, S. Emory, S.R. Probing Single Molecules and Single Nanoparticles by Surface-Enhanced Raman Scattering. Science 1997;275:1102-1106.
[7] Michaels, A.M. Jiang, J. Brus, L. Ag Nanocrystal Junctions as the Site for Surface-Enhanced Raman Scattering of Single Rhodamine 6G Molecules. J. Phys. Chem. B 2000;104:11965-11971.
[8] García-Martín, A. Ward, D.R. Natelson, D. Cuevas, J.C. Field enhancement in subnanometer metallic gaps. Phys. Rev. B 2011;83:193404-193404-4.
[9] Nien, L.W. Lin, S.C. Chao, B.K. Chen, M.J. Li, J.H. Hsueh, C.H. Giant Electric Field Enhancement and Localized Surface Plasmon Resonance by Optimizing Contour Bowtie Nanoantennas. J. Phys. Chem. C 2013;117:25004-25011.
[10] Hao E. Schatz, G.C. Electromagnetic fields around silver nanoparticles and dimers. J. Chem. Phys. 2004;120:357-366.
[11] Yurtsever A. Zewail, A.H. Direct Visualization of Near-Fields in Nanoplasmonics and Nanophotonics. Nano Lett. 2012;12:3334-3338.
[12] Herink, G. Solli, D.R. Ropers, C. Field-driven photoemission from nanostructures quenches the quiver motion. Nature 2012;483:190-193.
[13] Grubisic, A. Ringe, E. Cobley, C.M. Xia, Y. Marks, L.D. Van Duyne, R.P. Nesbitt, D.J. Plasmonic Near-Electric Field Enhancement Effects in Ultrafast Photoelectron Emission: Correlated Spatial and Laser Polarization Microscopy Studies of Individual Ag Nanocubes. Nano Lett. 2012;12:4823-4829.
[14] Dombi, P. Hörl, A. Rácz, P. Márton, I. Trügler, A. Krenn, J.R. Hohenester, U. Ultrafast Strong-Field Photoemission from Plasmonic Nanoparticles. Nano Lett. 2013;13:674-678.
[15] Einstein A. Über einen die Erzeugung und Verwandlung des Lichtes betreffenden heuristischen Gesichtspunkt. Ann. Phys. 1905;17:132-148.
[16] Keldysh, L.V. Ionization in the Field of a Strong Electromagnetic Wave. Sov. Phys. JETP 1965;20:1307-1314.
[17] Zherebtsov, S. Fennel, T. Plenge, J. Antonsson, E. Znakovskaya1, I. Wirth, A. Herrwerth, O. Süßmann, F. Peltz, C. Ahmad, I. Trushin, S.A. Pervak, V. Karsch, S. Vrakking, M.J.J.J. Langer, B. Graf, C. Stockman, M.I. Krausz, F. Rühl, E. and Kling M.F. Controlled near field enhanced electron acceleration from dielectric nanospheres with intense few cycle laser fields. Nat. Phys.2011;7:656-662
[18] Süßmann F. Seiffert, L. Zherebtsov, S. Mondes, V. Stierle, J. Arbeiter, M. Plenge, J. Rupp, P. Peltz, C. Kessel, A. Trushin, S.A. Ahn, B. Kim, D. Graf, C. Rühl, E. Kling M.F. Fennel, T. Field propagation-induced directionality of carrier-envelope phase-controlled photoemission from nanospheres. Nat. Commun. 2015;6:7944-7953
[19] Passig, J. Irsig, R. Truong, N.X. Fennel, Th. Tiggesbäumker, J. Meiwes-Broer, K.H. Nanoplasmonic electron acceleration in silver clusters studied by angular-resolved electron spectroscopy. New J. Phys. 2012;14:085020-085020-13.
[20] Davidovits, P. Egger, M.D. Scanning Laser Microscope. Nature 1969;223:831-831.
[21] Haberland, H. Mail, M. Mossier, M. Oiang, Y. Reiners, T. Thurner, Y. Filling of micron-sized contact holes with copper by energetic cluster impact. J. Vac. Sci. Technol. A. 1994;12:2925-2930.
[22] de Heer, W.A. The physics of simple metal clusters: experimental aspects and simple models. Rev. Mod. Phys. 1993;65:611-676.
[23] Wegner, K. Piseri, P. Tafreshi, H.V. Milani, P. Cluster beam deposition: a tool for nanoscale science and technology. J. Phys. D: Appl. Phys. 2006;39:R439–R459.
[24] Polking, M.J. Umbach, C.C. Radiation-induced surface conductivity in an alkaline-earth boroaluminosilicate glass measured with elevated-temperature scanning probe microscopy. J. Am. Ceram. Soc. 2005;88:2442–2446.
[25] Kreibig, U. Vollmer, M. Optical Properties of Metal Clusters. Springer, Berlin, 1995.
[26] Dulkeith, E. Niedereichholz, T. Klar, T.A. Feldmann, J. von Plessen, G. Gittins, D.I. Mayya, K.S. Caruso, F. Plasmon emission in photoexcited gold nanoparticles. Phys Rev. B. 2004;70:205424-205424-4.
[27] Fennel, Th. Döppner, T. Passig, J. Schaal, Ch. Tiggesbäumker, J. Meiwes-Broer, K.H. Plasmon-Enhanced Electron Acceleration in Intense Laser Metal-Cluster Interactions. Phys. Rev. Lett. 2007;98:143401-143401-4.
[28] Fang, Z. Zhen, Y.Z. Neumann, O. Polman, A. García de Abajo, F.J. Nordlander, P. Halas, N.J. Evolution of Light-Induced Vapor Gen-

eration at a Liquid-Immersed Metallic Nanoparticle. Nano Lett. 2013;13:1736-1742.
[29] Lukianova-Hleb,E. Hu, Y. Latterini, L. Tarpani, L. Lee, S. Drezek, R.A. Hafner, J.H. Lapotko, D.O. Plasmonic Nanobubbles as Transient Vapor Nanobubbles Generated around Plasmonic Nanoparticles. ACS Nano 2010;4:2109–2123.
[30] Boustead, I. Charlesby, A. Thermoluminescence in polyethylene. I. Electron traps. Proc. Roy. Soc. Lond. A. 1970;316:291-302.
[31] Charlesby, A. Partridge, R.H. The thermoluminescence of irradiated polyethylene and other polymers. Proc. Roy. Soc. Lond. A., 1963;271:170-187.
[32] Linkens, A. Vanderschueren, J. Experimental studies on the relationship between thermoluminescence and molecular relaxation processes in polymers. Journal of Electrostatics, 1977;3:149-154.
[33] Boustead, I, Thermoluminescence in polyethylene: II. Dose kinetics. Proc. Roy. Soc. Lond. A, 1970;318:459-471.
[34] Nyswander R.E. Cohn, B. Measurement of Thermoluminescence of glass exposed to light. J. Opt. Soc. A 1930;20:131-136.
[35] Johns H.E, Laughlin J.S. Interaction of radiation with matter.In: Hine G, Brownell G, eds. Radiation Dosimetry. New York, NY: Academic Press; 1956;49.
[36] Thompson, A.C. Vaughan, D. [Eds.], X-ray Data Booklet, second ed., Lawrence Berkeley National Laboratory, Berkeley, 2001.
[37] Herz, R.H. The Recording of Electron Tracks in Photographic Emulsions. Phys. Rev. 1949;75:479-485.
[38] Hofer, K.G. Biophysical Aspects of Auger Processes. Acta Oncologica 1996;35:189-196.
[39] Egerton, R.F.; Electron energy-loss spectroscopy in the TEM. Rep. Prog. Phys. 2009;72:016502-25.
[40] Hovington, P. Druiin, D. Gauvin, R. CASINO: A new Monte Carlo code in C language for electron beam interaction —part I: Description of the program. Scanning 1997;19:1–14.
[41] National Institute of Standards and Technology, estar database
[42] Herink, G. Solli, D.R. Ropers, C. Field-driven photoemission from nanostructures quenches the quiver motion. Nature 2012;483:190-193.
[43] Muskens, O. Christofilos, D. Del Fatti, N. Vallée, F. Optical response of a single noble metal nanoparticle. J. Opt. A: Pure Appl. Opt. 2006;8:S264–S272.
[44] Corkum, Plasma Perspective on Strong-Field Multiphoton Ionisation. Phys. Rev. Lett. 1993;71:1994-1997
[45] Saalman, U. Rost, J.M. Rescattering for Extended Atomic Systems. Phys. Rev. Lett. 2008;100: 133006-130007-4
[46] Fennel, Th. Meiwes-Broer, K.-H. Tiggesbäumker, J. Reinhard P.-G. Dinh P. M. and Suraud E. Laser-driven nonlinear cluster dynamics. Rev. Mod. Phys. 2010:82;1793-1842
[47] Herrmann, L.O. Valev, V.K. Tserkezis, C. Barnard, J.S. Kasera, S. Scherman, O.A. Aizpurua, J. Baumberg, J.J. Threading plasmonic nanoparticle strings with light. Nat. Commun. 2014;5:4568-4568-6.